# TEN MILLION-ATOM INGAAS EMBEDDED QUANTUM DOT ELECTRON $G$ FACTOR CALCULATIONS USING SEMI-EMPIRICAL PSEUDOPOTENTIALS

A DISSERTATION SUBMITTED TO

THE GRADUATE SCHOOL OF ENGINEERING AND SCIENCE

OF BILKENT UNIVERSITY

IN PARTIAL FULFILLMENT OF THE REQUIREMENTS FOR

THE DEGREE OF

DOCTOR OF PHILOSOPHY

IN

PHYSICS

By

Mustafa Kahraman

October 2022

Ten million-atom InGaAs Embedded Quantum Dot Electron $g$ factor Calculations Using Semi-Empirical Pseudopotentials

By Mustafa Kahraman

October 2022

We certify that we have read this dissertation and that in our opinion it is fully adequate, in scope and in quality, as a dissertation for the degree of Doctor of Philosophy.

Ceyhun Bulutay(Advisor)

Mehmet Özgür Oktel

Ahmet Keleş

Oğuz Gülseren

Engin Durgun

Approved for the Graduate School of Engineering and Science:

Orhan Arıkan
Director of the Graduate School

# ABSTRACT

## TEN MILLION-ATOM INGAAS EMBEDDED QUANTUM DOT ELECTRON $G$ FACTOR CALCULATIONS USING SEMI-EMPIRICAL PSEUDOPOTENTIALS

Mustafa Kahraman
Ph.D. in Physics
Advisor: Ceyhun Bulutay
October 2022

Quantum technologies rely on key capabilities such as electron spin control over the full-Bloch sphere, generation of indistinguishable single photons, or entangled photon pairs. For all these purposes, arguably the most established semiconductor structure currently is the self-assembled InGaAs quantum dots (QDs). In this thesis, electron ground state $g$ tensors of embedded InGaAs QDs are calculated employing an atomistic empirical pseudopotential method. Computed QDs have varied size, shape, indium molar fraction but uniform strain. The components of the $g$ tensor do not show appreciable deviation even though the shape is anisotropic for some of the studied QDs. Universality is observed when family of $g$ factor curves is plotted with respect to energy gap which generalizes the findings of a recent study under more restricted conditions. Our work expands its applicability to alloy QDs with different shapes, and finite confinement putting it on a more realistic foundation by allowing penetration to the matrix material. Our regression model shows that the effect of magnetic field on the electron in an InGaAs QD will be the minimal when the so-called, $s$-shell optical transition energy is around 1.13 eV. Furthermore, low indium molar fraction is unfavorable in terms of $g$ factor tunability. Our findings could be beneficial in the fabrication of $g$-near-zero QDs or other desired $g$ values aimed for spintronic or electron spin resonance applications.

*Keywords:* g factor, g tensor, quantum dot, atomistic electronic structure, InGaAs.

# ÖZET

# ON MILYON ATOMLU, GÖMÜLÜ INGAAS KUANTUM NOKTALARIN YARI-DENEYSEL POTANSIYELLERLE ELEKTRON $G$ ÇARPANI HESAPLAMALARI

Mustafa Kahraman
Fizik, Doktora
Tez Danışmanı: Ceyhun Bulutay
Ekim 2022

Kuantum teknolojileri elektron spininin tüm Bloch küresi üzerinde kontrolü, ayırt edilemeyen tek foton üretimi, ya da dolanık foton çifti gibi yeteneklere gereksinim duyar. Bütün bu amaçlar için en iyi yarıiletken yapı şu anda InGaAs kuantum noktalardır. Bu tezde farklı şekile, boyuta, indiyum yoğunluğuna ve tekdüze gerinmeye sahip gömülü InGaAs kuantum noktaların temel elektron durumlarının $g$ tensörleri atom düzeyinde deneysel potansiyel yöntemiyle hesaplanmıştır. Bazı kuantum nokta şekillerinin anizotropik olmasına rağmen bulunan tensör değerlerinin birbirinden kayda değer bir farkı yoktur. $g$ çarpanı - enerji aralığı eğrileri çizdirildiğinde $g$ çarpanının evrenselliği daha önceki bir çalışmada kısıtlı parametreler için gösterilmişti. Bizim çalışmamız bu evrenselliğin alaşım InGaAs kuantum noktalarda ve çevreleyen matrisine nüfuz ettiği daha gerçekçi durumlarda görüldüğünü ortaya koymaktadır. Regresyon modelimiz optik geçiş enerjisinin 1.13 eV olduğu durumda manyetik alanın elektron üzerindeki etkisinin en az olduğunu söylemektedir. Ayrıca, az indiyum yoğunluğundaki kuantum noktaların $g$ çarpanı ayarlanabilirliklerinin düşük olduğu bulunmuştur. Çalışmamız sıfıra yakın $g$ çarpanlı kuantum nokta üretimi ya da başka arzulanan $g$ çarpanlı kuantum noktaların spintronik veya elektron spin yankısı çalışmaları için yararlı olacaktır.

*Anahtar sözcükler*: g çarpanı, g tensor, kuantum nokta, atomsal elekronik yapı, InGaAs.

# Acknowledgement

I would like to express my graditute to my advisor Ceyhun Bulutay for his support, patience and kindness.Without his guidance this thesis would not be realized.

I thank the members of my thesis monitering committee Mehmet Özgür Oktel and Ahmet Keleş for allocating time and discussions. Also, I thank jury members Oğuz Gülseren and Engin Durgun.

I thank my friend Ekrem Taha Güldeste for his support and invaluable friendship for all these years. Also, I thank my old colleagues and friends Ahmed Ouf and Murod Bahovadinov for their friendship.

I thank Bilkent University and Department of Physics for the financial support.

Lastly, without the support of my family I would be doomed. I cannot thank enough to my mother Gülcan and my brother Mete Han.

This work was funded by Türkiye Bilimsel ve Teknolojik Araştırma Kurumu (TUBITAK) under Project No. 116F075. The numerical calculations reported in this paper were partially performed at TÜBITAK ULAKBIM, High Performance and Grid Computing Center (TRUBA resources).

# Contents

# List of Figures

# List of Tables

# Chapter 1

# Introduction

$g$ factor is the coupling constant which determines the strength of the interaction of a charge with an external magnetic field. For a *free* electron according to Dirac equation $g = 2$, in solids mainly due to spin-orbit coupling it gets renormalized, which is denoted as $g^*$ [3, 4]. For the nanostructures like quantum dots (QDs), the confinement further renormalizes the $g$ factor by altering the orbital contribution inside a heterogeneous environment [5], therewithal offers electrical tunability [6, 7, 8, 9, 10]. One prominent structure is self-assembled InGaAs QDs, where some quantum technological breakthroughs have been shown, such as indistinguishable single-photon sources [11], also on demand [12], spin-resolved resonance fluorescence [13], spin-photon interface [14], entangled photon pairs [15], entanglement swapping [16], as well as simultaneous antibunching and squeezing [17]. The electron spin resonance (ESR) has also been shown in embedded InGaAs QDs but it has not been reproduced since [18]. This is quite important as it would have allowed direct magnetic field control of the carrier spin over the full Bloch sphere.

## 1.1 Tunability of g

$g$-near-zero ($g^* \sim 0$) QDs which would result in intriguing physics are also worth considering for number of reasons. External magnetic field affects nuclear spins three orders of magnitude less than the free electrons due to their Landé factor ratio [19]. Therefore, ESR and nuclear magnetic resonance (NMR) frequencies would mismatch by that amount. $g$-near-zero QDs reduce this mismatch which allows for electron-nucleus counter spin flips. Comparable to Hartman-Hahn double resonance [20, 21, 22], this can enable strong coupling between electron and nuclear spin bath. From a fundamental scientific perspective, $g$-near-zero can allow a spin-density wave state where the spins are perpendicular to the magnetic field [23], and spin texture of skyrmionic excitations [24]. Electric gating can change the sign of $g^*$ which promote controlled spin rotation [6, 25]. Furthermore, $g$-near-zero allows for quantum state transfer between a resident electron spin qubit in a QD and a flying photon qubit [26]. Therefore, a better grasp of the variables that influence the $g$ factor in InGaAs QDs, is very beneficial for many research paths.

## 1.2 Current Challenges

The experimental studies that characterize the $g$ factor [27, 28, 29, 30, 1, 31, 32, 33, 34, 2] suffer from inability to extract the sign using magnetoluminescence-based measurements [28, 29, 8, 1, 31, 10, 33, 34], magnetocapacitance [30], and photocurrent spectroscopy [2]. Another challenge is the lack of accurate structural information, such as the alloy composition, shape, and consequently the strain profile of the single QD. The efforts for incorporating the structural information to the model that agree with both the cross-sectional scanning tunneling microscopy and spectroscopy measurements [35, 36] do not clear the ambiguity as they would ignore the decaying indium concentration around the periphary of the QD and the wetting layer [37, 38].

On the theoretical side, although more refined calculations exist [39, 40, 41, 42] $g$ factor calculations usually employ $k \cdot p$ model which generally neglects the structural information [43, 44, 45, 46, 47]. As mentioned in these works, $g$ factor has direct dependence to the energy gap which renders lack of structural information not crucial. These works verify the Roth-Lax-Zwerdling bulk expression for $g$ factor [48] in nanostructures. Studying only compound QDs, a recent tight-binding calculation validated that bulk term comprises the majority of the contribution to the $g$ factor [49]. These statements surely warrant additional theoretical research, ideally using an atomistic electronic structure method that may provide better insights into $g^*$ of alloy InGaAs QDs [27, 28, 29, 6, 8, 9, 1, 31].

## 1.3 This Work

In this work, we study $g$ factor of $In_xGa_{1-x}As$ QDs where the core is under homogeneous compressive strain [50, 51, 52]. There are a few choices for the host material such as GaAs with band gap of 1.52 eV which is the most common one, $In_xAl_{1-x}As$ with 2 eV [53] and $(In_xGa_{1-x})_2O_3$ with 5 eV band gaps [54]. Here, these wide range of band gap materials in mind, the host material is chosen to be an artificial material with a band gap that is sufficient to confine the $s$-shell ground state electron. The QDs that were studied have spherical and hydrophobic and lens geometries which are cut from a sphere with respect to [111] axis. Alloy profile of the QDs are chosen as uniform with various mole fractions considered.

For the QDs targeted in this Thesis, the total number of atoms inside the nanostructures including the host material is around 10 million. Therefore, it is important to use an efficient electronic structure method for the calculations. For this purpose we used linear combination of bulk bands (LCBB) method which can deal with such large number of atoms with low computational cost [55]. This method has been previously employed for the linear optical response [56], third-order nonlinear optics [57], electroabsorption [58], and coherent population transfer [59] in nanocrystals and for electronic structure [60] and ballistic transport [61] in nanowire structures.

Our findings verify aforementioned tight-binding study where universality of $g^*$ with respect to energy gap has been reported [49]. Additionally, the regression model that we have found applies to not only compound InAs but also InGaAs alloy QDs with various shapes where the wavefunction penetrates to the host material as in the real-world samples due to finite confinement. This can be valuable for controlled ESR in InGaAs QDs [18] or for avoiding it. Precise frequency should be known for achieving ESR, hence the $g$ factor. Our fit can be used for predicting $g$ factor from energy gap without having any information on indium molar fraction, shape or other structural characteristics. Furthermore, we have found that if electron spin qubit should be protected from the magnetic effects ($g^* \sim 0$) [62], transition energy of the InGaAs QDs should be around 1.13 eV according to our regression model [63].

This thesis is organized as follows: In Chapter 2 theory of LCBB technique, $g$ factor and spin-orbit interaction is described. Our results on $g$ factor for numerous QD structures are presented in Chapter 3 and conclusion in Chapter 4. The computational details are given in Appendix.

# Chapter 2

# Theory

## 2.1 Linear Combination of Bulk Bands

For an atomistic electronic structure calculation, a large basis set such as plane waves or localized Gaussian orbitals increases the computational cost in order for the accuracy not to be compromised. The linear combination of bulk bands (LCBB) technique solves the necessity of large basis set problem by the use of small, physically intiutive basis set for a restricted energy window of interest [55]. Bulk Bloch functions of the constituent materials of the nanostructure is used to form the basis set. Therefore, expanding the $j^{th}$ stationary state wave function by (of say a QD) is given by

$$\psi_j(\mathbf{r}) = \frac{1}{\sqrt{N}} \sum_{n,\mathbf{k},\mu} C_{n\mathbf{k}}^{\mu,j} u_{n\mathbf{k}}^{\mu}(\mathbf{r}) e^{i\mathbf{k}\cdot\mathbf{r}}, \tag{2.1}$$

where $N$ is the number of unit cells of the supercell of the nanostructure, $n$ is the index of the bulk band, $\mathbf{k}$ is the wavevector in the first Brillouin zone, $\mu$ is the material index, and $C_{n\mathbf{k}}^{\mu,j}$ is the expansion coefficient. $u_{n\mathbf{k}}^{\mu}(\mathbf{r})$ is the cell-periodic part of the Bloch functions of each constituent material $\mu$ which can be expanded as a Fourier series as

$$u_{n\mathbf{k}}^{\mu}(\mathbf{r}) = \frac{1}{\sqrt{\Omega_0}} \sum_{\mathbf{G}} B_{n\mathbf{k}}^{\mu}(\mathbf{G}) e^{i\mathbf{G}\cdot\mathbf{r}},$$

where $\mathbf{G}$ is the reciprocal lattice vector, and $\Omega_0$ is the volume of the primitive cell [4]. The expansion coefficients $B^{\mu}_{n\mathbf{k}}(\mathbf{G})$ come from the diagonalization of the bulk Hamiltonian at each $\mathbf{k}$ point for a constituent material $\mu$.

The total of kinetic energy and crystal potential give the single-particle Hamiltonian of a nanostructure. The crystal potential of the atomistic environment comes from the empirical pseudopotentials [64]

$$\begin{aligned}\mathcal{H} &= \mathcal{T} + \mathcal{V}_{\text{xtal}} \\ &= -\frac{\hbar^2\nabla^2}{2m_0} + \sum_{\mu,\mathbf{R}_l,\alpha} W^{\mu}_{\alpha}(\mathbf{R}_l)\, \upsilon^{\mu}_{\alpha}(\mathbf{r}-\mathbf{R}_l-\mathbf{d}^{\mu}_{\alpha})\,,\end{aligned}$$

where $m_0$ is the free electron mass, $\mathbf{R}_l$ is the direct lattice vector pointing to each primitive cell $l$, and $\mathbf{d}^{\mu}_{\alpha}$ is the position vector of the basis atom $\alpha$ of material $\mu$. $W^{\mu}_{\alpha}(\mathbf{R}_l)$ is the weight and takes the value of 1 if atom $\alpha$ of material $\mu$ is present at $\mathbf{R}_l+\mathbf{d}^{\mu}_{\alpha}$, zero otherwise. $\upsilon^{\mu}_{\alpha}$ is the local screened spherical atomic pseudopotential [64].

Energy eigenvalues $E_j$ and coefficients $C^{\mu,j}_{n\mathbf{k}}$ are determined by the generalized eigenvalue equation

$$\sum_{n,\mathbf{k},\mu}\langle n'\mathbf{k}'\mu'|\mathcal{T}+\mathcal{V}_{\text{xtal}}|n\mathbf{k}\mu\rangle\, C^{\mu,j}_{n\mathbf{k}} = E_j \sum_{n,\mathbf{k},\mu} C^{\mu,j}_{n\mathbf{k}}\langle n'\mathbf{k}'\mu'|n\mathbf{k}\mu\rangle\,,$$

where the each matrix elements can be written as

$$\langle n'\mathbf{k}'\mu'|n\mathbf{k}\mu\rangle = \delta_{\mathbf{k},\mathbf{k}'}\sum_{\mathbf{G}}\left[B^{\mu'}_{n'\mathbf{k}}(\mathbf{G})\right]^* B^{\mu}_{n\mathbf{k}}(\mathbf{G})\,,$$

$$\langle n'\mathbf{k}'\mu'|\mathcal{T}|n\mathbf{k}\mu\rangle = \delta_{\mathbf{k},\mathbf{k}'}\sum_{\mathbf{G}}\frac{\hbar^2|\mathbf{k}+\mathbf{G}|^2}{2m_0}\left[B^{\mu'}_{n'\mathbf{k}}(\mathbf{G})\right]^* B^{\mu}_{n\mathbf{k}}(\mathbf{G})\,,$$

$$\begin{aligned}\langle n'\mathbf{k}'\mu'|\mathcal{V}_{\text{xtal}}|n\mathbf{k}\mu\rangle = \quad & \textstyle\sum_{\mathbf{G},\mathbf{G}'}\left[B^{\mu'}_{n'\mathbf{k}'}(\mathbf{G}')\right]^* B^{\mu}_{n\mathbf{k}}(\mathbf{G}) \\ & \times \textstyle\sum_{\mu'',\alpha}\mathcal{V}^{\mu''}_{\alpha}(|\mathbf{k}+\mathbf{G}-\mathbf{k}'-\mathbf{G}'|) \\ & \times \mathcal{W}^{\mu''}_{\alpha}(\mathbf{k}-\mathbf{k}')e^{-i(\mathbf{k}+\mathbf{G}-\mathbf{k}'-\mathbf{G}')\cdot\mathbf{d}^{\mu''}_{\alpha}}\,.\end{aligned}$$

Here, $\mathcal{V}^{\mu''}_{\alpha}$ and $\mathcal{W}^{\mu''}_{\alpha}$ are the Fourier transforms of atomic pseudopotentials and

the weight functions

$$\mathcal{V}_{\alpha}^{\mu''}(|\mathbf{k}+\mathbf{G}-\mathbf{k}'-\mathbf{G}'|) = \frac{1}{\Omega_0}\int v_{\alpha}^{\mu''}(\mathbf{r})e^{i(\mathbf{k}+\mathbf{G}-\mathbf{k}'-\mathbf{G}')\cdot\mathbf{r}}d^3r, \tag{2.2}$$

$$\mathcal{W}_{\alpha}^{\mu}(\mathbf{k}-\mathbf{k}') = \sum_j W_{\alpha}^{\mu''}(\mathbf{R}_j)e^{i(\mathbf{k}-\mathbf{k}')\cdot\mathbf{R}_j}. \tag{2.3}$$

## 2.2 Spin-Orbit Interaction

Up until now, we have considered only the spinless Hamiltonian. The spin-orbit interaction can be added by following Hybertsen and Louie [65]. Spin-orbit interaction Hamiltonian is given as

$$\mathcal{H}_{SO} = \sum_{\ell=1}^{\infty} |\ell\rangle\, V_{\ell}^{SO}(r)\boldsymbol{\ell}\cdot\boldsymbol{\sigma}\,\langle\ell|\ , \tag{2.4}$$

where, $\ell$ is the orbital angular momentum, $V_{\ell}^{SO}(r)$ is the nonlocal radial spin-orbit potential, and $\boldsymbol{\sigma}$ is the Pauli spin operator. Instead of all $\ell$, we limit ourselves with the dominant $p$ ($\ell = 1$) component. With this simplification, we write the matrix elements for the spin-orbit interaction as

$$\begin{aligned}\langle s,\mathbf{K}|\,\mathcal{H}_{SO}\,|s',\mathbf{K}'\rangle &= -i\,\langle s|\,\boldsymbol{\sigma}\,|s'\rangle\cdot\Bigg[12\pi\frac{\mathbf{K}\times\mathbf{K}'}{KK'} \\ &\quad\times V_{\ell=1}^{SO}(K,K')\Bigg]S(\mathbf{K}'-\mathbf{K})\ ,\end{aligned} \tag{2.5}$$

where $\mathbf{K} = \mathbf{k}+\mathbf{G}$, $\mathbf{K}' = \mathbf{k}+\mathbf{G}'$, $|s\rangle$ is a spinor state, $S(\mathbf{K}'-\mathbf{K})$ is the bulk structure factor. $V_{\ell}^{SO}(K,K')$ can be written as

$$V_{\ell}^{SO}(K,K') = \int_0^{\infty}\frac{dr}{\Omega_0}r^2 j_{\ell}(Kr)\ V_{\ell}^{SO}(r)\ j_{\ell}(K'r)\ , \tag{2.6}$$

where $j_{\ell}$ is the spherical Bessel function of the first kind and $V_{\ell}^{SO}(r)$ is chosen as a Gaussian function [66] and its amplitude being a fit parameter. $V_{\ell}^{SO}(K,K')$ is calculated once, and stored in a look-up table for further use.

## 2.3 $g$ Factor

The coupling between an external magnetic field and a nanostructure is anisotropic which renders $g$ factor to be rank-2 tensor $\overleftrightarrow{g}$, which has nine linearly independent components [43]. The Zeeman Hamiltonian which describes the interaction is

$$\mathcal{H}_Z = \frac{1}{2}\mu_B \boldsymbol{\sigma} \cdot \overleftrightarrow{g} \cdot \mathbf{B}, \tag{2.7}$$

where $\mu_B$ is the Bohr magneton. The formulation of $\overleftrightarrow{g}$ corresponds to incorporating spin-orbit interaction as a first-order perturbation [67, 4]. With respect to the matrix elements between two confined states $n$ and $j$, this bulk formulation can be applied to QDs

$$\mathbf{p}_{nj} = \frac{(2\pi)^3}{\Omega_{\rm SC}} \int_{\rm SC} \psi_n^*(\mathbf{r})\ \mathbf{p}\ \psi_j(\mathbf{r})\ d^3r\,, \tag{2.8}$$

$$\mathbf{h}_{nj} = \frac{(2\pi)^3}{\Omega_{\rm SC}} \int_{\rm SC} \psi_n^*(\mathbf{r})\ \mathbf{h}\ \psi_j(\mathbf{r})\ d^3r\,, \tag{2.9}$$

where the integrations are over the volume of the supercell ($\Omega_{\rm SC}$), $\mathbf{p}$ is the momentum operator, and $\mathbf{h}$ is an operator related to spin-orbit as $\mathcal{H}_{SO} = \mathbf{h} \cdot \boldsymbol{\sigma}$; see, Eq. (2.4). The $g$ factor for a chosen state $n$ can be found as

$$\begin{aligned} \overleftrightarrow{g}_n &= 2\overleftrightarrow{I} + \frac{2}{i\hbar^2 m_0} {\sum_{jl}}' \frac{1}{\omega_{nj}} \left[ \frac{(\mathbf{h}_{jl} - \mathbf{h}_{lj})(\mathbf{p}_{nj} \times \mathbf{p}_{ln})}{\omega_{jl}} \right. \\ &\quad \left. + \frac{(\mathbf{h}_{ln} - \mathbf{h}_{nl})(\mathbf{p}_{nj} \times \mathbf{p}_{jl})}{\omega_{nl}} \right], \end{aligned} \tag{2.10}$$

where $\overleftrightarrow{I}$ is the identity matrix. The prime over the summation denotes $j \neq l$, and $\omega_{nj} = (E_n - E_j)/\hbar$. With some algebraic manipulations, we can arrive at Roth's bulk $g$ factor expression [67]

$$\begin{aligned} \overleftrightarrow{g}_n &= 2\overleftrightarrow{I} + \frac{2}{i\hbar^2 m_0} {\sum_{jl}}' \frac{1}{\omega_{nj}\omega_{nl}} \left( \mathbf{h}_{nj}\mathbf{p}_{jl} \times \mathbf{p}_{ln} \right. \\ &\quad \left. + \mathbf{h}_{jl}\mathbf{p}_{nj} \times \mathbf{p}_{ln} + \mathbf{h}_{ln}\mathbf{p}_{nj} \times \mathbf{p}_{jl} \right), \end{aligned} \tag{2.11}$$

where we choose $n$ and $j$ as the nanostructure's confined states as opposed to bulk.

# Chapter 3

# Results[1]

## 3.1 Wavefunctions of InAs QDs

To highlight the atomistic nature of our electronic structure approach, we would like to start with a small album of wavefunctions of typical QDs. They illustrate the energetic hierarchy of low-lying electron states subject to band mixing and quantum confinement. In Fig. 3.1 we present an atomistic wavefunction and its envelope function of an InAs QD that are calculated employing LCBB. In Fig. 3.2 and Fig. 3.3 conduction band envelopes of freestanding spherical and hemispherical InAs QDs with 10 nm diameter are shown, respectively. Due to anisotropy of hemispherical QD, the wavefunctions get mixed in orbital angular momentum. Mixing is more pronounced in lens shaped QDs that we will eloborate in the remainder of the chapter.

[1] **The results in this chapter are published in Ref. [63]**

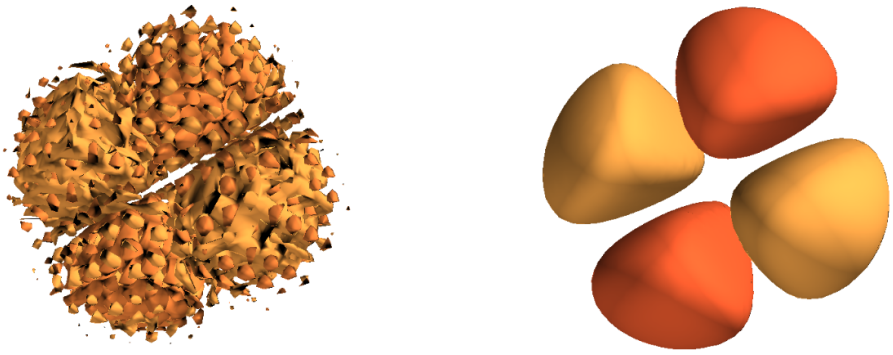

Figure 3.1: Atomistic wavefunction of InAs QD (left) and its extracted envelope (right).

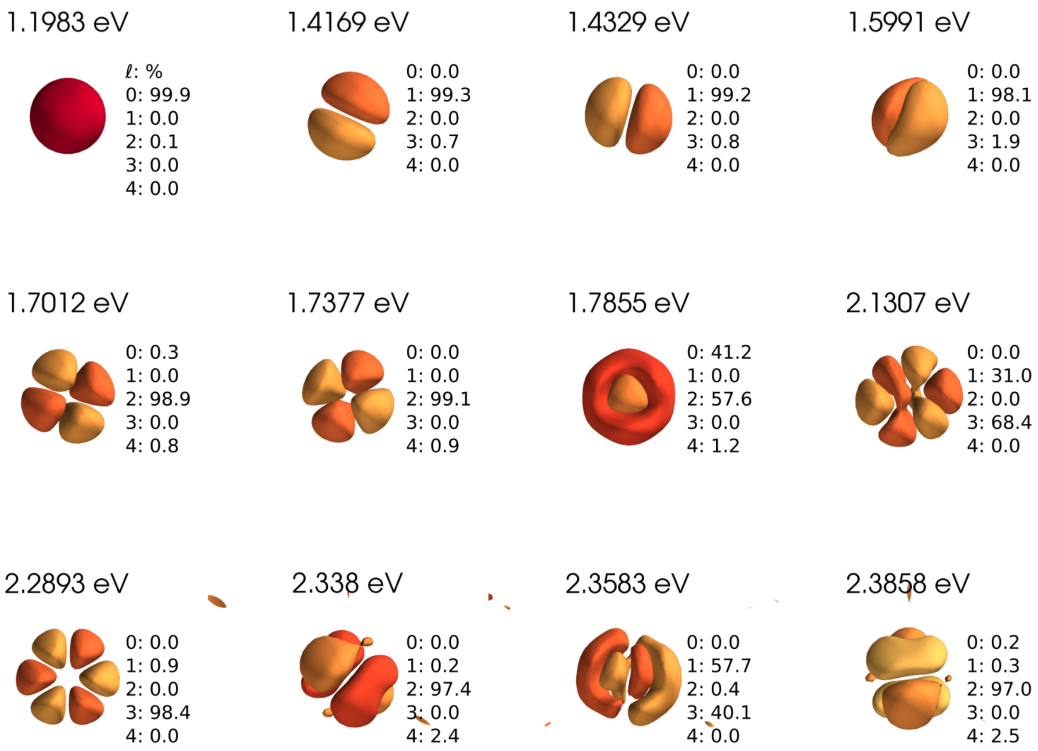


Figure 3.2: Conduction band wavefunction envelopes of freestanding spherical InAs QD with 10 nm diameter.

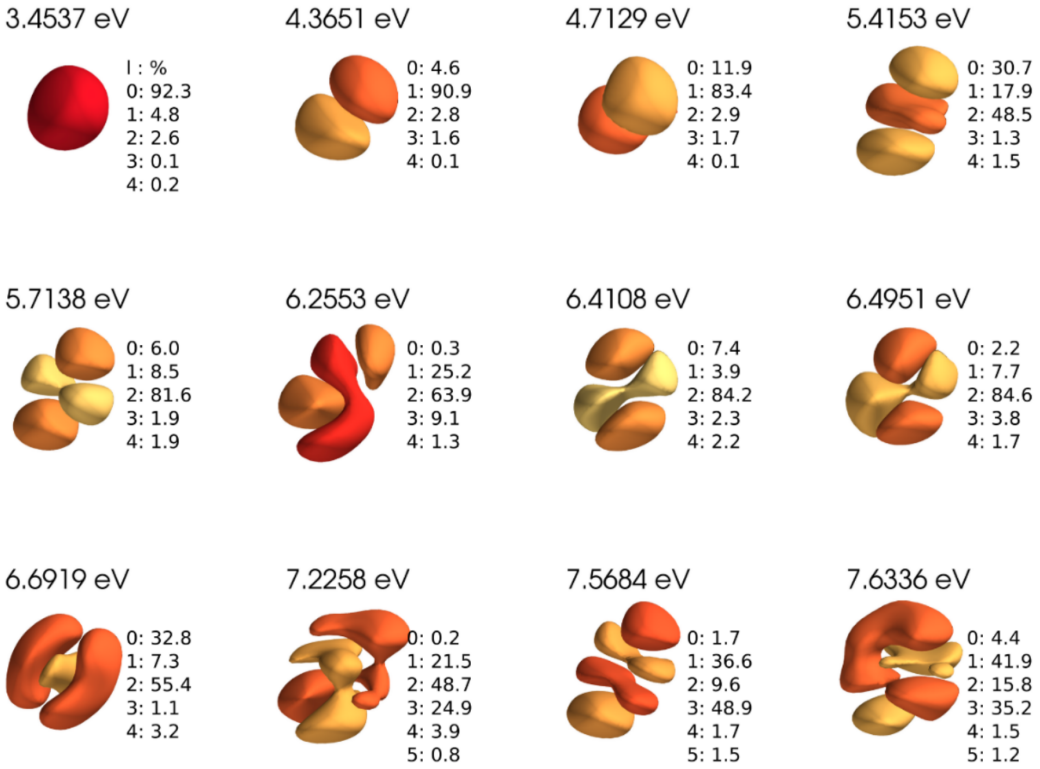


Figure 3.3: Conduction band wavefunction envelopes of freestanding hemispherical InAs QD with 10 nm diameter.

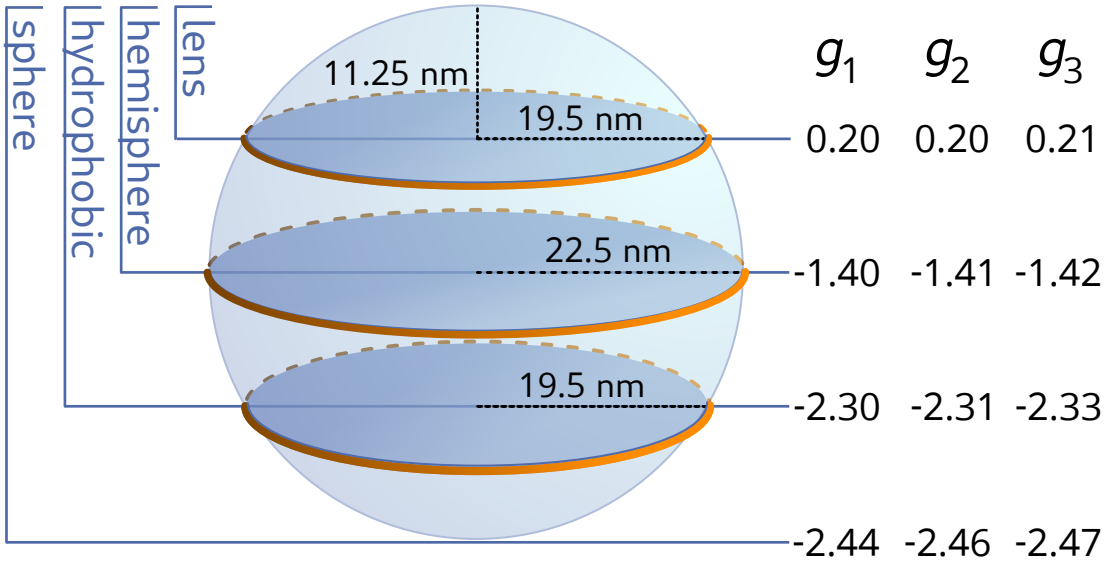


Figure 3.4: Principal $\overleftrightarrow{g}$ values for spherical, hydrophobic-contact-angle, hemispherical, lens shaped QDs under uniform compressive strain of $\epsilon_{xx} = \epsilon_{yy} = \epsilon_{zz} = -0.02$. Non-spherical shapes were cut by (111) planes from the spherical QD.

## 3.2 Geometrical Construction of QDs and $g$ Tensor

In this section we are looking at embedded spherical InAs QD of 45 nm diameter which is under hydrostatic strain of $\epsilon_H = -0.06$ or i.e. 2% compressive strain. In Fig. 3.4, the spherical QD is cut by (111) planes such that the cut QDs correspond to a hydrophobic-contact-angle, hemispherical and lens shaped QDs. We are interested in the variation in principal values of $\overleftrightarrow{g}$. Confinement increases by the decreasing volume of the QD which alters the $g^*$ from -2.47 to 0.21, while $g^* \sim 0$ corresponds to a lens shaped QD with bigger height than the one given in Fig 3.4. The anisotropy between principal values of $\overleftrightarrow{g}$ is greater in spherical QD with an absolute difference of 0.03 even though other QDs have anisotropic shapes. This negligible difference shows the accuracy of our results so that only the major principal value will be given in the remaining plots.

## 3.3 Indium Mole Fraction Dependence

We consider spherical, hemispherical and lens shaped $In_xGa_{1-x}As$ QDs under -2% uniform compressive strain with fixed diameters of about 46 nm and and for the lens shaped QD with a height of 11-12 nm. By varying indium molar fraction we will examine $g$ factor and the energy gap $E_g$ between highest occupied molecular orbital (HOMO) and lowest unoccupied molecular orbital (LUMO). In Fig. 3.5 both the $g^*$ and the energy gap decreases as the indium molar fraction increases. In Fig. 3.5(a) $g^*$ decreases drastically for the indium rich QDs which shows increase in $g$-tunability. Also, the sign of $g^*$ changes in this region.

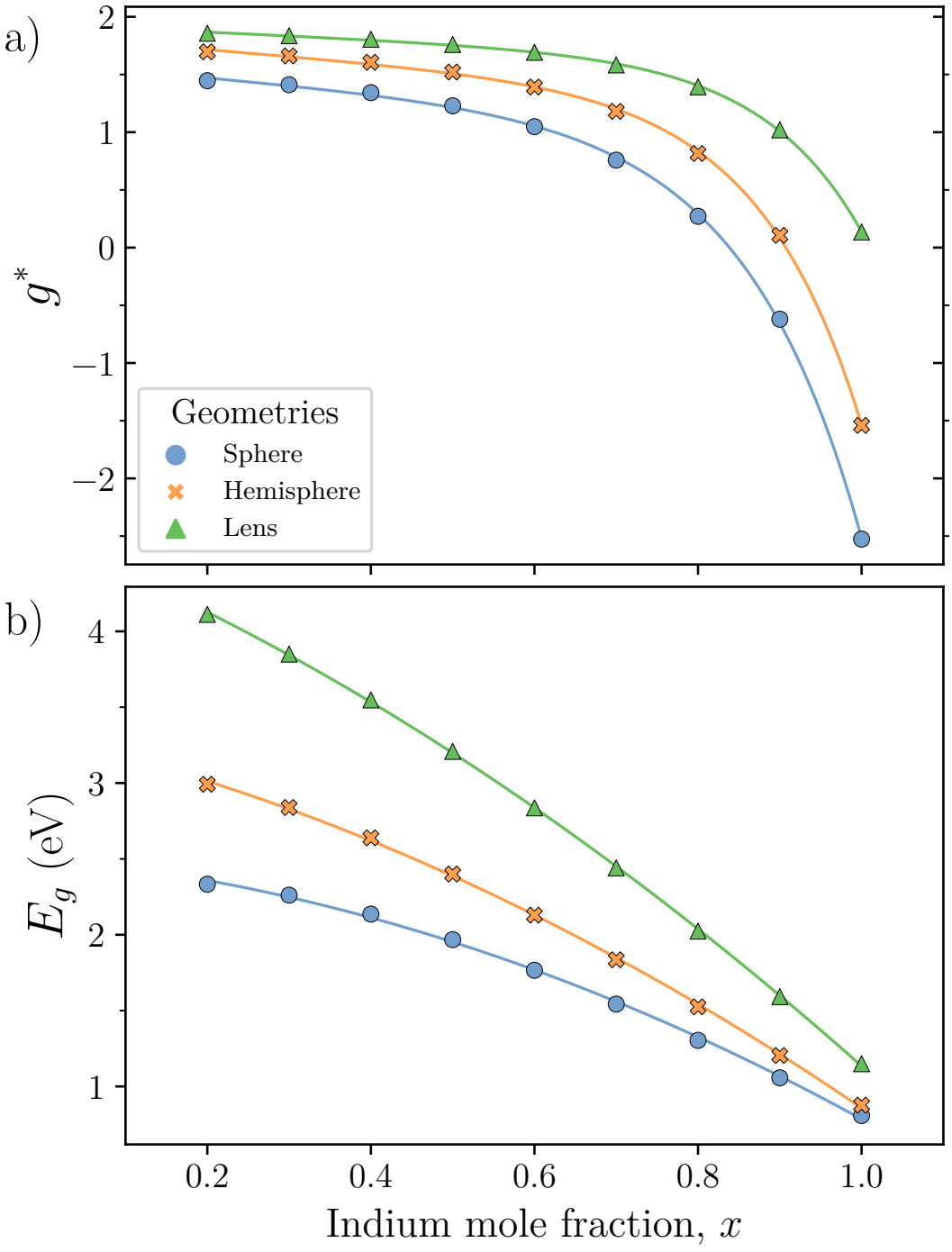


Figure 3.5: (a) $g$ factor, and (b) HOMO-LUMO energy gap, $E_g$ of the spherical, hemispherical and lens-shaped $In_xGa_{1-x}As$ QDs under $-2\%$ homogeneous strain as a function of the indium molar fraction. QDs have the same diameter of 46 nm, and the height of the lens QDs are about 11-12 nm. Lines are to guide the eye.

## 3.4 Dimensional Dependence in Lens QDs

In this section and the next, dimensional dependence to $g$ factor in lens shaped QDs is studied. In Fig. 3.6 we fix the aspect ratio to 0.2 which is the height over diameter of the lens QDs under compressive strain and show family of curves for varying indium molar fraction. Looking at the QDs having the same indium molar fractions, we conclude that due to increased strain energy gap increases in Fig. 3.6(b). This is due to the negative deformation potentials of the InAs and GaAs [68]. Energy gap comes into play in Eqs. (2.11) in the denominator. Therefore, the increase in energy gap means less contribution to the $g$ factor as in Fig. 3.6(a). The same conclusion can also be reached by the similarity between conduction band effective mass formula and the $g$ factor expression, increase of energy gap decreases the effective mass [69]. Furthermore, spin-orbit interaction contribution increases with increasing indium molar fraction which means contribution to $g$ factor also increases. For the lower indium molar fractions, $g$ factor being almost size independent also holds true for Fig. 3.5.

In Fig. 3.7 we keep basal diameter constant at 35 nm and height was varied. As same as previous discussions, $g$ factor decreases with decreasing energy gap but this time the change in $g$ factor larger due to increasing aspect ratio. $g$-near-zero corresponds to an InAs QD. In Fig. 3.7 we see data points for ($x = 0.5,\ \epsilon_{ii} = -0.01$) and ($x = 0.8,\ \epsilon_{ii} = -0.03$) overlaps with each other in accordance with a universal behavior.

## 3.5 Universality with respect to gap energy

In Fig. 3.8 we plot all of the $g$ factor data in Figs. 3.5, 3.6, 3.7 with respect to energy gap $E_g$ which could even be improved by addition of excitonic binding energies [58]. We see that all the data that corresponds to various strain conditions, alloy fractions, dimensions, and host material follow a universal curve which is

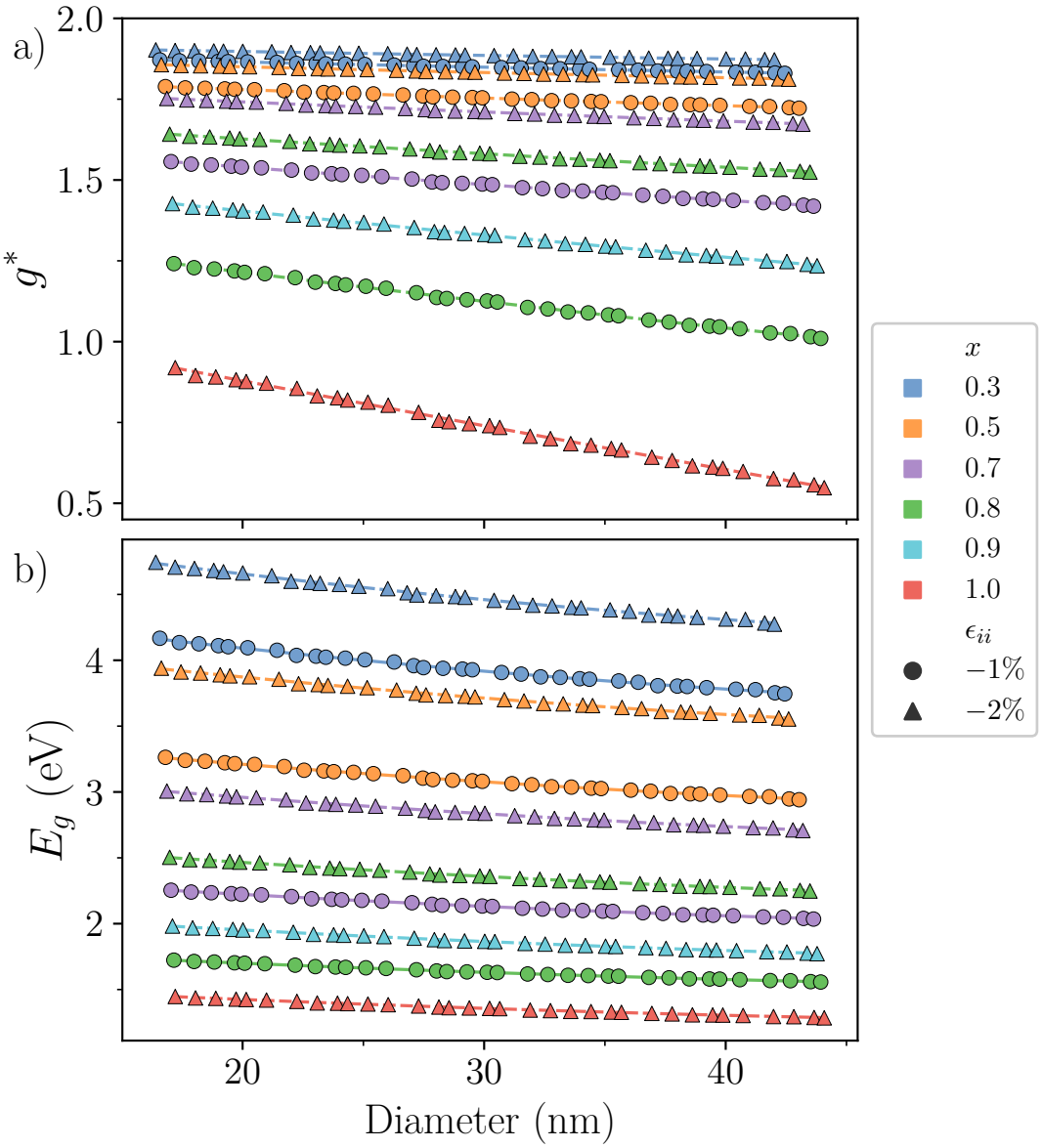


Figure 3.6: (a) $g$ factor, and (b) HOMO-LUMO energy gap, $E_g$ with respect to the diameter of the lens QD. All QDs have fixed aspect ratio of $h/D = 0.2$ for different indium mole fraction, and strain values. Dashed lines are to guide the eye.

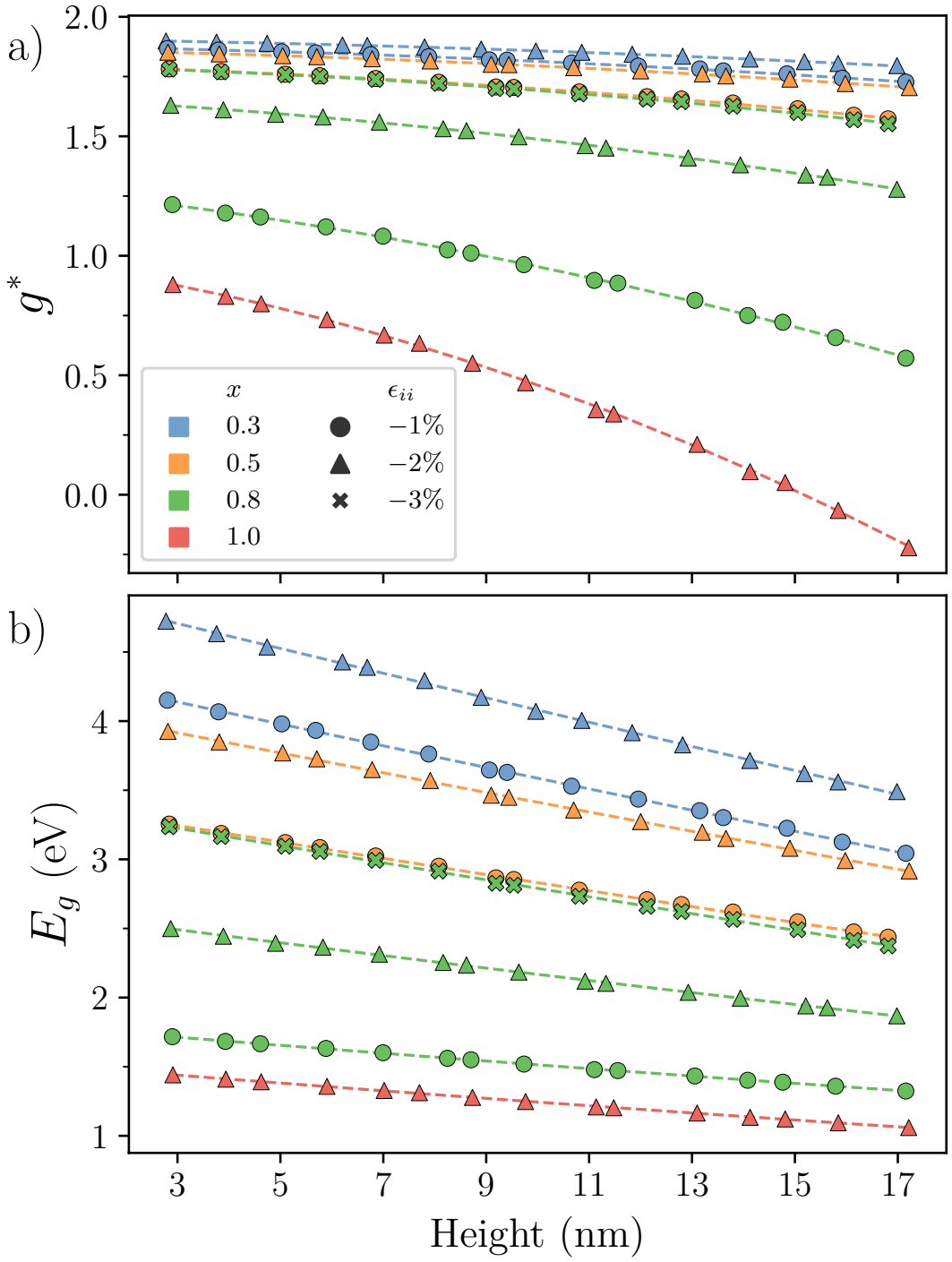


Figure 3.7: (a) $g$ factor, and (b) HOMO-LUMO energy gap, $E_g$ with respect to the height of the lens QD for a fixed basal diameter of 35 nm. The family of curves are for different indium mole fraction, and strain values. Dashed lines are to guide the eye.

the bulk expression for the $g$ factor [48, 44]

$$g^*(E_g) = 2 - \frac{2.06}{E_g(E_g - 0.22)}\,, \tag{3.1}$$

where $E_g$ is in eV. This is the main result of this Thesis. This expression, while supporting the previous findings in Ref. [49], also extends it for the cases of different settings that our data provides that are stated above.

## 3.6 Utility of the Universal Expression

The regression curve in Eq. 3.1 allows us to predict the case where $g \sim 0$ to be around 1.13 eV where the QD would be least prone to magnetic field. Photocurrent spectroscopy, magnetocapacitance and magnetoluminescence experiments that can extract $g$ factor cannot resolve its sign. In Fig. 3.8(a) two experimental data is given where $g$ factor - energy gap pairs for an InGaAs lens QD with a diameter of 30 nm and height of $7 - 8$ nm [1] designated by pink star and for another with pink cross [2]. Making use of the fit function in Eq. 3.1, we can determine their signs to be positive. Furthermore, Eq. 3.1 can be used for engineering $g$ factor [29, 70] to a desired value by tuning the energy gap.

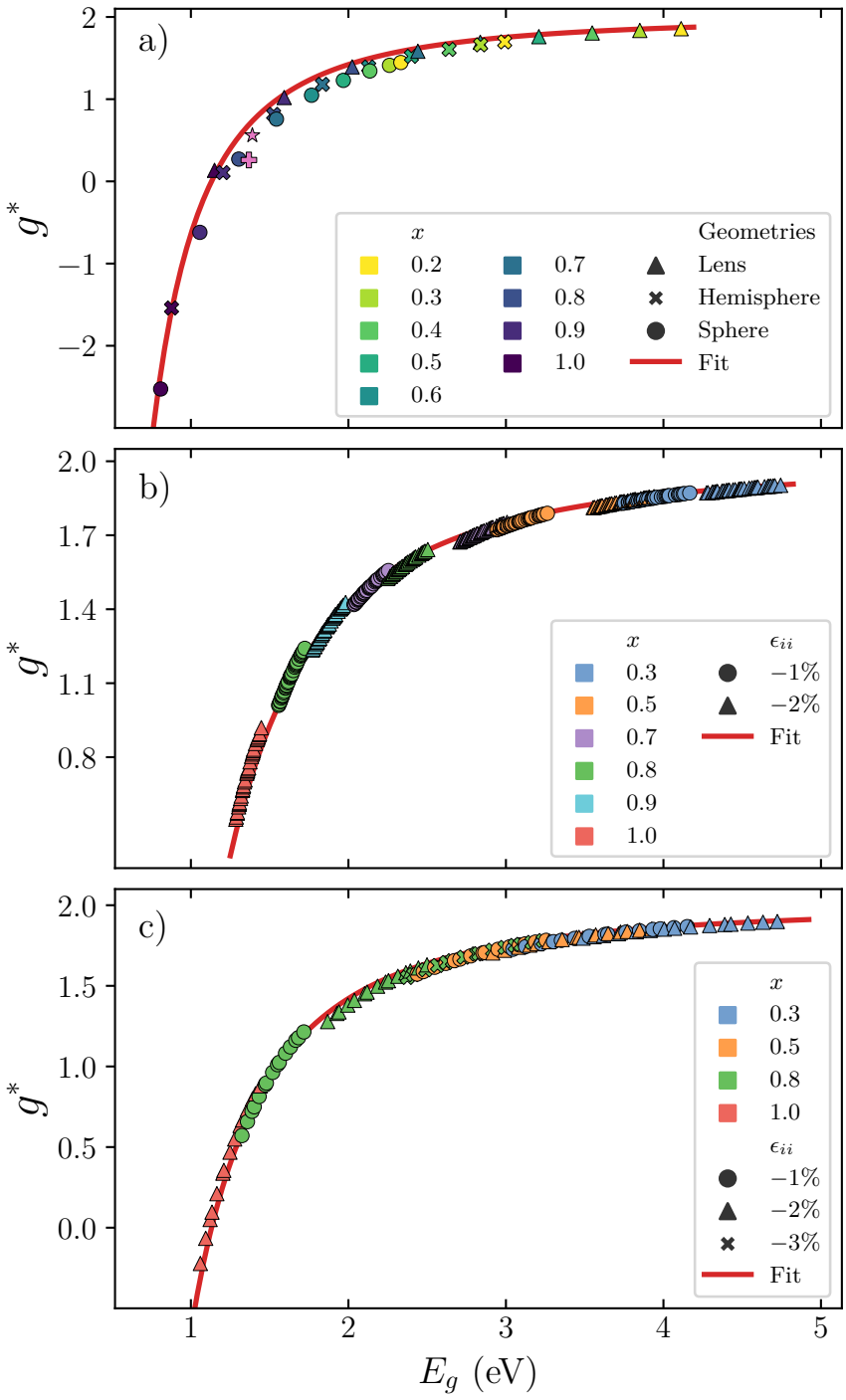


Figure 3.8: $g$-factor's universal behavior obtained when the data for (a) different geometries in Fig. 3.5, (b) diameter series in Fig. 3.6, and (c) height series at $D = 35$ nm in Fig. 3.7, are re-plotted with respect to $E_g$. Two other literature data points included in (a) (see the text), as star [1] and cross [2] symbols in pink. All fitted curves follow Eq. (3.1).

# Chapter 4

# Conclusion

Spintronics, which primarily relies on spin as opposed to electrical charge, gives unique opportunities for highly sophisticated quantum applications. Being optically active, the direct gap semiconductors, and in particular InGaAs based QDs are unsurpassed for spin-dependent quantum technologies. Some quantum phenomena exhibited on this system are single photon sources, dynamical nuclear spin polarization, optically detected nuclear magnetic resonance, spin-photon interface as well as entanglement swapping. Despite of all these impressive achievements, as a major shortcoming, reproducible ESR that can be singled out from the background spin noise has not been unambiguously demonstrated for embedded QDs.

In this Thesis, $g$ tensors of embedded InGaAs QDs having various shapes, sizes, indium molar fractions and strain profiles are calculated by employing an atomistic electronic structure method. The analysis of the computed $g$ factors reveals general trends. Our findings can be valuable for achieving $g$-near-zero InGaAs QDs or ESR-based quantum logic operations. Our study verifies a recent tight-binding article on universal behavior of $g$ factor with respect to energy gap in compound QDs [49]. We demonstrated that this universality also covers alloy InGaAs QDs with different strain profiles and shapes where the penetration to the host material is allowed.

## 4.1 Suggestions as Follow-up Directions

On the order of 10-million atom QD g-factor computation is rather an ambitious task. This inevitably obliged us to make a number of simplifying assumptions in our atomistic model, mainly posed by its prohibitive computational budget. In this final part, we would like to list several directions in which our research can be improved from both methodological as well as materials aspects. Foremost, the LCBB technique is non-selfconsistent, unlike the state-of-the-art electronic structure codes like VASP [71]. As a matter of fact, we owe this simplification to reaching 10 million-atom scale with modest computational powers. Nevertheless, it brings adverse issues such as tuning the pseudopotential energy line-ups (hence additional ad hoc parameters) under strain or interfaces etc, which would not be the case for a self- consistent approach. Therefore, bringing a computationally-cheap self-consistency to LCBB is always welcomed. Another limitation that we ought to introduce was assuming a homogeneous strain in QDs which enabled the use of standard FFT routines. In realistic InGaAs QDs as relaxed by molecular static force fields [52], an inhomogeneous atomistic strain profile exists that necessitate non-uniform FFT [72, 73], or linearized handling of inhomogeneous strain using standard FFT [55] . As another concern in LCBB we should also note its non-monotonic $k$-grid convergence.

Regarding specifically the $g$-factor calculation, as opposed to the generalized Roth expression [67] as we used in this Thesis, an alternative is to make use of geometric phase concepts [74]. Here, the numerical problem arising from the random phases introduced to eigenvectors by eigensolvers need to be confronted. On the materials side, $g$-factor of few-percentage antimony containing InGaAs QDs would be interesting which would bring wider tunability for spintronic applications.

# Bibliography


[1] A. Schwan, B.-M. Meiners, A. Henriques, A. Maia, A. Quivy, S. Spatzek, S. Varwig, D. Yakovlev, and M. Bayer, "Dispersion of electron g-factor with optical transition energy in (in, ga) as/gaas self-assembled quantum dots," *Applied Physics Letters*, vol. 98, no. 23, p. 233102, 2011.

[2] S. Wu, K. Peng, X. Xie, J. Yang, S. Xiao, F. Song, J. Dang, S. Sun, L. Yang, Y. Wang, *et al.*, "Electron and hole g tensors of neutral and charged excitons in single quantum dots by high-resolution photocurrent spectroscopy," *Physical Review Applied*, vol. 14, no. 1, p. 014049, 2020.

[3] Y. Yafet, "g factors and spin-lattice relaxation of conduction electrons," in *Solid state physics*, vol. 14, pp. 1–98, Elsevier, 1963.

[4] J. Callaway, *Quantum theory of the solid state*. Academic press, 2013.

[5] M. T. Sandoval, J. L. Padilla, A. F. da Silva, E. d. A. e Silva, and G. La Rocca, "Mesoscopic g-factor renormalization for electrons in iii-v interacting nanolayers," *Physical Review B*, vol. 98, no. 7, p. 075312, 2018.

[6] T. Nakaoka, S. Tarucha, and Y. Arakawa, "Electrical tuning of the g factor of single self-assembled quantum dots," *Physical Review B*, vol. 76, no. 4, p. 041301, 2007.

[7] Y. K. Kato and D. D. Awschalom, "Electrical manipulation of spins in nonmagnetic semiconductors," *Journal of the Physical Society of Japan*, vol. 77, no. 3, pp. 031006–031006, 2008.

[8] F. Klotz, V. Jovanov, J. Kierig, E. Clark, D. Rudolph, D. Heiss, M. Bichler, G. Abstreiter, M. Brandt, and J. Finley, "Observation of an electrically tunable exciton g factor in ingaas/gaas quantum dots," *Applied Physics Letters*, vol. 96, no. 5, p. 053113, 2010.

[9] J. Pingenot, C. E. Pryor, and M. E. Flatté, "Electric-field manipulation of the landé g tensor of a hole in an in 0.5 ga 0.5 as/gaas self-assembled quantum dot," *Physical Review B*, vol. 84, no. 19, p. 195403, 2011.

[10] M. Taylor, P. Spencer, E. Clarke, E. Harbord, and R. Murray, "Tuning exciton g-factors in inas/gaas quantum dots," *Journal of Physics D: Applied Physics*, vol. 46, no. 50, p. 505105, 2013.

[11] C. Santori, D. Fattal, J. Vučković, G. S. Solomon, and Y. Yamamoto, "Indistinguishable photons from a single-photon device," *nature*, vol. 419, no. 6907, pp. 594–597, 2002.

[12] Y.-M. He, Y. He, Y.-J. Wei, D. Wu, M. Atatüre, C. Schneider, S. Höfling, M. Kamp, C.-Y. Lu, and J.-W. Pan, "On-demand semiconductor single-photon source with near-unity indistinguishability," *Nature nanotechnology*, vol. 8, no. 3, pp. 213–217, 2013.

[13] A. Nick Vamivakas, Y. Zhao, C.-Y. Lu, and M. Atatüre, "Spin-resolved quantum-dot resonance fluorescence," *Nature Physics*, vol. 5, no. 3, pp. 198–202, 2009.

[14] S. Yılmaz, P. Fallahi, and A. Imamoğlu, "Quantum-dot-spin single-photon interface," *Physical review letters*, vol. 105, no. 3, p. 033601, 2010.

[15] R. M. Stevenson, A. J. Hudson, A. J. Bennett, R. J. Young, C. A. Nicoll, D. A. Ritchie, and A. J. Shields, "Evolution of entanglement between distinguishable light states," *Physical review letters*, vol. 101, no. 17, p. 170501, 2008.

[16] W. Gao, P. Fallahi, E. Togan, J. Miguel-Sánchez, and A. Imamoglu, "Observation of entanglement between a quantum dot spin and a single photon," *Nature*, vol. 491, no. 7424, pp. 426–430, 2012.

[17] C. H. Schulte, J. Hansom, A. E. Jones, C. Matthiesen, C. Le Gall, and M. Atatüre, "Quadrature squeezed photons from a two-level system," *Nature*, vol. 525, no. 7568, pp. 222–225, 2015.

[18] M. Kroner, K. M. Weiss, B. Biedermann, S. Seidl, S. Manus, A. W. Holleitner, A. Badolato, P. M. Petroff, B. D. Gerardot, R. J. Warburton, *et al.*, "Optical detection of single-electron spin resonance in a quantum dot," *Physical review letters*, vol. 100, no. 15, p. 156803, 2008.

[19] B. Urbaszek, X. Marie, T. Amand, O. Krebs, P. Voisin, P. Maletinsky, A. Högele, and A. Imamoglu, "Nuclear spin physics in quantum dots: An optical investigation," *Reviews of Modern Physics*, vol. 85, no. 1, p. 79, 2013.

[20] S. Hartmann and E. Hahn, "Nuclear double resonance in the rotating frame," *Physical Review*, vol. 128, no. 5, p. 2042, 1962.

[21] P. London, J. Scheuer, J.-M. Cai, I. Schwarz, A. Retzker, M. B. Plenio, M. Katagiri, T. Teraji, S. Koizumi, J. Isoya, *et al.*, "Detecting and polarizing nuclear spins with double resonance on a single electron spin," *Physical review letters*, vol. 111, no. 6, p. 067601, 2013.

[22] G.-Q. Liu, Q.-Q. Jiang, Y.-C. Chang, D.-Q. Liu, W.-X. Li, C.-Z. Gu, H. C. Po, W.-X. Zhang, N. Zhao, and X.-Y. Pan, "Protection of centre spin coherence by dynamic nuclear spin polarization in diamond," *Nanoscale*, vol. 6, no. 17, pp. 10134–10139, 2014.

[23] S. R. Julian and M. R. Norman, "Genetics and g-factors," *Nature Physics*, vol. 7, no. 3, pp. 191–192, 2011.

[24] V. Mitrović, M. Horvatić, C. Berthier, S. Lyon, and M. Shayegan, "Nmr study of large skyrmions in al 0.13 ga 0.87 as quantum wells," *Physical Review B*, vol. 76, no. 11, p. 115335, 2007.

[25] A. Ulhaq, Q. Duan, E. Zallo, F. Ding, O. G. Schmidt, A. Tartakovskii, M. Skolnick, and E. A. Chekhovich, "Vanishing electron g factor and long-lived nuclear spin polarization in weakly strained nanohole-filled gaas/algaas quantum dots," *Physical Review B*, vol. 93, no. 16, p. 165306, 2016.

[26] M. Kuwahara, T. Kutsuwa, K. Ono, and H. Kosaka, "Single charge detection of an electron created by a photon in a g-factor engineered quantum dot," *Applied Physics Letters*, vol. 96, no. 16, p. 163107, 2010.

[27] M. Bayer, A. Kuther, A. Forchel, A. Gorbunov, V. Timofeev, F. Schäfer, J. Reithmaier, T. Reinecke, and S. Walck, "Electron and hole g factors and exchange interaction from studies of the exciton fine structure in in 0.60 ga 0.40 as quantum dots," *Physical Review Letters*, vol. 82, no. 8, p. 1748, 1999.

[28] T. Nakaoka, T. Saito, J. Tatebayashi, and Y. Arakawa, "Size, shape, and strain dependence of the g factor in self-assembled in (ga) as quantum dots," *Physical Review B*, vol. 70, no. 23, p. 235337, 2004.

[29] T. Nakaoka, T. Saito, J. Tatebayashi, S. Hirose, T. Usuki, N. Yokoyama, and Y. Arakawa, "Tuning of g-factor in self-assembled in (ga) as quantum dots through strain engineering," *Physical Review B*, vol. 71, no. 20, p. 205301, 2005.

[30] T. M. Alegre, F. Hernández, A. Pereira, and G. Medeiros-Ribeiro, "Landé g tensor in semiconductor nanostructures," *Physical review letters*, vol. 97, no. 23, p. 236402, 2006.

[31] A. Schwan, B.-M. Meiners, A. Greilich, D. Yakovlev, M. Bayer, A. Maia, A. Quivy, and A. Henriques, "Anisotropy of electron and hole g-factors in (in, ga) as quantum dots," *Applied Physics Letters*, vol. 99, no. 22, p. 221914, 2011.

[32] L. Sapienza, R. Al-Khuzheyri, A. Dada, A. Griffiths, E. Clarke, and B. D. Gerardot, "Magneto-optical spectroscopy of single charge-tunable inas/gaas quantum dots emitting at telecom wavelengths," *Physical Review B*, vol. 93, no. 15, p. 155301, 2016.

[33] H. Tholen, J. Wildmann, A. Rastelli, R. Trotta, C. Pryor, E. Zallo, O. Schmidt, P. Koenraad, and A. Y. Silov, "Strain-induced g-factor tuning in single ingaas/gaas quantum dots," *Physical Review B*, vol. 94, no. 24, p. 245301, 2016.

[34] H. Tholen, J. Wildmann, A. Rastelli, R. Trotta, C. Pryor, E. Zallo, O. Schmidt, P. Koenraad, and A. Y. Silov, "Active tuning of the g-tensor in ingaas/gaas quantum dots via strain," *Physical Review B*, vol. 99, no. 19, p. 195305, 2019.

[35] V. Mlinar and A. Zunger, "Spectral barcoding of quantum dots: Deciphering structural motifs from the excitonic spectra," *Physical Review B*, vol. 80, no. 3, p. 035328, 2009.

[36] V. Mlinar, M. Bozkurt, J. Ulloa, M. Ediger, G. Bester, A. Badolato, P. Koenraad, R. Warburton, and A. Zunger, "Structure of quantum dots as seen by excitonic spectroscopy versus structural characterization: Using theory to close the loop," *Physical Review B*, vol. 80, no. 16, p. 165425, 2009.

[37] A. Giddings, J. Keizer, M. Hara, G. Hamhuis, H. Yuasa, H. Fukuzawa, and P. Koenraad, "Composition profiling of inas quantum dots and wetting layers by atom probe tomography and cross-sectional scanning tunneling microscopy," *Physical Review B*, vol. 83, no. 20, p. 205308, 2011.

[38] J. Keizer, M. Jo, T. Mano, T. Noda, K. Sakoda, and P. Koenraad, "Structural atomic-scale analysis of gaas/algaas quantum wires and quantum dots grown by droplet epitaxy on a (311) a substrate," *Applied Physics Letters*, vol. 98, no. 19, p. 193112, 2011.

[39] C. J. Delerue and M. Lannoo, *Nanostructures: theory and modeling*. Springer Science & Business Media, 2013.

[40] M. Usman, "Atomistic theoretical study of electronic and polarization properties of single and vertically stacked elliptical inas quantum dots," *Physical Review B*, vol. 86, no. 15, p. 155444, 2012.

[41] C. E. Pryor and M.-E. Pistol, "Atomistic $k \cdot p$ theory," *Journal of Applied Physics*, vol. 118, no. 22, p. 225702, 2015.

[42] A. Mittelstädt, A. T. Ludwig, S. T. Jagsch, A. Schliwa, *et al.*, "Efficient electronic structure calculations for extended systems of coupled quantum dots using a linear combination of quantum dot orbitals method," *Physical Review B*, vol. 103, no. 11, p. 115302, 2021.

[43] A. Kiselev, E. Ivchenko, and U. Rössler, "Electron g factor in one-and zero-dimensional semiconductor nanostructures," *Physical Review B*, vol. 58, no. 24, p. 16353, 1998.

[44] C. E. Pryor and M. E. Flatté, "Landé g factors and orbital momentum quenching in semiconductor quantum dots," *Physical Review Letters*, vol. 96, no. 2, p. 026804, 2006.

[45] R. Zielke, F. Maier, and D. Loss, "Anisotropic g factor in inas self-assembled quantum dots," *Physical Review B*, vol. 89, no. 11, p. 115438, 2014.

[46] K. Gawarecki, "Spin-orbit coupling and magnetic-field dependence of carrier states in a self-assembled quantum dot," *Physical Review B*, vol. 97, no. 23, p. 235408, 2018.

[47] A. Mielnik-Pyszczorski, K. Gawarecki, and P. Machnikowski, "Limited accuracy of conduction band effective mass equations for semiconductor quantum dots," *Scientific reports*, vol. 8, no. 1, pp. 1–12, 2018.

[48] L. M. Roth, B. Lax, and S. Zwerdling, "Theory of optical magneto-absorption effects in semiconductors," *Physical Review*, vol. 114, no. 1, p. 90, 1959.

[49] A. Tadjine, Y.-M. Niquet, and C. Delerue, "Universal behavior of electron g-factors in semiconductor nanostructures," *Physical Review B*, vol. 95, no. 23, p. 235437, 2017.

[50] F. Guffarth, R. Heitz, A. Schliwa, O. Stier, N. Ledentsov, A. Kovsh, V. Ustinov, and D. Bimberg, "Strain engineering of self-organized inas quantum dots," *Physical Review B*, vol. 64, no. 8, p. 085305, 2001.

[51] M. Usman, V. Tasco, M. T. Todaro, M. De Giorgi, E. P. O'Reilly, G. Klimeck, and A. Passaseo, "The polarization response in inas quantum dots: theoretical correlation between composition and electronic properties," *Nanotechnology*, vol. 23, no. 16, p. 165202, 2012.

[52] C. Bulutay, "Quadrupolar spectra of nuclear spins in strained in x ga 1- x as quantum dots," *Physical Review B*, vol. 85, no. 11, p. 115313, 2012.

[53] S. Golovynskyi, O. I. Datsenko, L. Seravalli, G. Trevisi, P. Frigeri, B. Li, D. Lin, and J. Qu, "Inas/ingaas quantum dots confined by inalas barriers for enhanced room temperature light emission: Photoelectric properties and deep levels," *Microelectronic Engineering*, vol. 238, p. 111514, 2021.

[54] H. Von Wenckstern, D. Splith, M. Purfürst, Z. Zhang, C. Kranert, S. Müller, M. Lorenz, and M. Grundmann, "Structural and optical properties of (in, ga) 2o3 thin films and characteristics of schottky contacts thereon," *Semiconductor Science and Technology*, vol. 30, no. 2, p. 024005, 2015.

[55] L.-W. Wang and A. Zunger, "Linear combination of bulk bands method for large-scale electronic structure calculations on strained nanostructures," *Physical Review B*, vol. 59, no. 24, p. 15806, 1999.

[56] C. Bulutay, "Interband, intraband, and excited-state direct photon absorption of silicon and germanium nanocrystals embedded in a wide band-gap lattice," *Physical Review B*, vol. 76, no. 20, p. 205321, 2007.

[57] H. Yıldırım and C. Bulutay, "Bound-state third-order optical nonlinearities of germanium nanocrystals embedded in a silica host matrix," *Physical Review B*, vol. 78, no. 11, p. 115307, 2008.

[58] C. Bulutay, M. Kulakci, and R. Turan, "Stark effect, polarizability, and electroabsorption in silicon nanocrystals," *Physical Review B*, vol. 81, no. 12, p. 125333, 2010.

[59] D. Gunceler and C. Bulutay, "dc-switchable and single-nanocrystal-addressable coherent population transfer," *Applied Physics Letters*, vol. 97, no. 24, p. 241909, 2010.

[60] U. Keleş, B. Liedke, K.-H. Heinig, and C. Bulutay, "Networks of silicon nanowires: A large-scale atomistic electronic structure analysis," *Applied Physics Letters*, vol. 103, no. 20, p. 203103, 2013.

[61] Ü. Keleş, A. Çakan, and C. Bulutay, "Disorder-free localization around the conduction band edge of crossing and kinked silicon nanowires," *Journal of Applied Physics*, vol. 117, no. 6, p. 064308, 2015.

[62] A. Bechtold, D. Rauch, F. Li, T. Simmet, P.-L. Ardelt, A. Regler, K. Müller, N. A. Sinitsyn, and J. J. Finley, "Three-stage decoherence dynamics of an electron spin qubit in an optically active quantum dot," *Nature Physics*, vol. 11, no. 12, pp. 1005–1008, 2015.

[63] M. Kahraman and C. Bulutay, "Electron ground state g factor in embedded ingaas quantum dots: An atomistic study," *Physical Review B*, vol. 103, no. 11, p. 115303, 2021.

[64] G. Bester, "Electronic excitations in nanostructures: an empirical pseudopotential based approach," *Journal of Physics: Condensed Matter*, vol. 21, no. 2, p. 023202, 2008.

[65] M. S. Hybertsen and S. G. Louie, "Spin-orbit splitting in semiconductors and insulators from the ab initio pseudopotential," *Physical Review B*, vol. 34, no. 4, p. 2920, 1986.

[66] A. Williamson, L. Wang, and A. Zunger, "Theoretical interpretation of the experimental electronic structure of lens-shaped self-assembled inas/gaas quantum dots," *Physical Review B*, vol. 62, no. 19, p. 12963, 2000.

[67] L. M. Roth, "g factor and donor spin-lattice relaxation for electrons in germanium and silicon," *Physical Review*, vol. 118, no. 6, p. 1534, 1960.

[68] A. Çakan, C. Sevik, and C. Bulutay, "Strained band edge characteristics from hybrid density functional theory and empirical pseudopotentials: Gaas, gasb, inas and insb," *Journal of Physics D: Applied Physics*, vol. 49, no. 8, p. 085104, 2016.

[69] Y. Peter and M. Cardona, *Fundamentals of semiconductors: physics and materials properties*. Springer Science & Business Media, 2010.

[70] G. Medeiros-Ribeiro, E. Ribeiro, and H. Westfahl Jr, "g-factor engineering and control in self-assembled quantum dots," *Applied Physics A*, vol. 77, no. 6, pp. 725–729, 2003.

[71] G. Kresse and J. Furthmüller, "Efficiency of ab-initio total energy calculations for metals and semiconductors using a plane-wave basis set," *Computational materials science*, vol. 6, no. 1, pp. 15–50, 1996.

[72] A. H. Barnett, J. Magland, and L. af Klinteberg, "A parallel nonuniform fast fourier transform library based on an "exponential of semicircle" kernel," *SIAM Journal on Scientific Computing*, vol. 41, no. 5, pp. C479–C504, 2019.

[73] A. H. Barnett, "Aliasing error of the exp($\beta$1- z2) kernel in the nonuniform fast fourier transform," *Applied and Computational Harmonic Analysis*, vol. 51, pp. 1–16, 2021.

[74] D. Vanderbilt, *Berry phases in electronic structure theory: electric polarization, orbital magnetization and topological insulators*. Cambridge University Press, 2018.

[75] M. Frigo, "Proc. 1999 acm sigplan conf. on programming language design and implementation," 1999.

[76] C. G. Van de Walle, "Band lineups and deformation potentials in the model-solid theory," *Physical review B*, vol. 39, no. 3, p. 1871, 1989.

[77] C. Pryor, "Eight-band calculations of strained inas/gaas quantum dots compared with one-, four-, and six-band approximations," *Physical Review B*, vol. 57, no. 12, p. 7190, 1998.

[78] M. Usman, H. Ryu, I. Woo, D. S. Ebert, and G. Klimeck, "Moving toward nano-tcad through multimillion-atom quantum-dot simulations matching experimental data," *IEEE Transactions on Nanotechnology*, vol. 8, no. 3, pp. 330–344, 2009.

# Appendix A

# Computational Details

We use empirical pseudopotentials for strained/natural InAs and GaAs that are fitted to band structures from hybrid density functional theory [68] where they are fitted with approximately 120 reciprocal lattice vectors up to an energy cut-off below about 10 Ry. To represent alloy $In_xGa_{1-x}As$ core, Vegard's law was used in mixing InAs and GaAs pseudopotentials. Experimental spin-orbit splittings are used to fit the spin-orbit interaction in the bulk InAs and GaAs which contributes to $g$ factor.

The sum in the $\overleftrightarrow{g}_n$ expression in Eq. (2.11) are over all QD states, but it is important to characterise the states that are close to the state $n$ in terms of energy which are dependent to the quality of the LCBB basis set. The basis set are constructed by employing top four valence bands and a lowest conduction band of the core/host materials under strain and without spin on a $5 \times 5 \times 5$ reciprocal space grid around the $\Gamma$ point. The LCBB sets that we use in this work accommodate around two thousand elements and we verified the convergence for the supercell dimensions of the nanostructures of interest.

Due to non-self-consistency of the emprirical psuedopotentials [64], an extra parameter was required for the alignment of the bulk bands under strain which

is implemented as a hydrostatic strain dependent pseudopotential

$$V(q;\epsilon) = [1 + \gamma\,\epsilon_H]\; V(q)\,, \tag{A.1}$$

where $\gamma$ is the fitting parameter and $\epsilon_H = \epsilon_{xx} + \epsilon_{yy} + \epsilon_{zz}$ is hydrostatic strain [66]. In our calculations lattice constant was chosen to be the same across the supercell which corresponds to a uniformly strained QD. Due to this simplification, choise of the basis sets gets easier and the use of fast Fourier transform (FFT) is allowed in Eq. (2.3) [75]. Due to the strain-dependent band gap, incorporating the existing theoretical and experimental band offset data [76, 77, 78] is still hard. The use of uniform lattice constant requires various artificial matrix materials where the lattice constant matches with that of strained core QD. Their band gap are between 1.52 eV (corresponds to GaAs) and 5 eV (corresponds to $\mathrm{In}_x\mathrm{Ga}_{1-x})_2\mathrm{O}_3$.

In reality, for an embedded InGaAs QD, the strain is position dependent due to relaxation [77, 66, 50]. For LCBB, this corresponds to using non-uniform FFT and bigger and richer basis set which increases computational cost significantly, even if we use optimized non-uniform FFT packages [72, 73]. That is why we have limited this work on various uniformly strained QDs where the uniform strain corresponds to average strain in a QD [50, 51, 52].